

Experimental and modelling results of the QUENCH-18 bundle experiment on air ingress, cladding melting and aerosol release

Juri Stuckert^{a,*}, Martin Steinbrueck^a, Jarmo Kalilainen^b, Terttaliisa Lind^b, Jonathan Birchley^c

^a Karlsruhe Institute of Technology (KIT), Germany

^b Paul Scherrer Institut (PSI), Switzerland

^c Reactor Physics and Thermal-Hydraulics Organization, Paul Scherrer Institut (PSI) Street, Forschungsstrasse, 111, 5232 Villigen, Switzerland

ABSTRACT

The primary aims of the QUENCH-18 bundle test were to examine the oxidation of M5® claddings in air/steam mixture following a limited pre-oxidation in steam, and to achieve a long period of oxygen and steam starvation to promote interaction with the nitrogen. Additionally, the QUENCH-18 experiment investigated the effects of the presence of two Ag-In-Cd control rods, and two pressurized unheated rod simulators (6 MPa, He). The twenty low-pressurized heater rods (0.23 MPa, similar to the system pressure) were Kr-filled. In a first transient, the bundle was heated in an atmosphere of flowing argon and superheated steam by electrical power increase to the peak cladding temperature of 1400 K. During this heat-up, claddings of the two pressurized rods were burst at temperature of 1045 K. The attainment of 1400 K marked the start of the pre-oxidation stage to achieve a maximum cladding oxide layer thickness of about 80 µm. In the air ingress stage, the steam and argon flows were reduced, and air was injected. The first Ag-In-Cd aerosol release was registered at 1350 K and was dominated by Cd bearing aerosols. Later in the transient, a significant release of Ag was observed. A strong temperature escalation started in the middle of the air ingress stage. During the air ingress stage, a period of oxygen starvation occurred, which was followed by almost complete steam consumption and partial consumption of the nitrogen indicating formation of zirconium nitrides under oxygen starvation conditions. The temperatures continued to increase and stabilized at the melting temperature of Zr bearing materials until water injection. Almost immediately after the start of reflood there was a temperature excursion, leading to maximum measured temperatures of about 2430 K. Final quench was achieved after about 800 s. A significant quantity of hydrogen was generated during the reflood (238 g). Nitrogen release (>54 g) due to re-oxidation of nitrides was also registered. Residual zirconium nitrides were observed in the bundle middle. The metallographic investigations of the bundle show strong cladding oxidation and Zr melt formation. The Zr melt relocated downwards to the lower bundle part was strongly oxidized. Partially oxidized Zr-bearing melt was found down to elevation 160 mm; this elevation was the lowest with evidence of relocated pellet material. At the bundle bottom, only frozen metallic melt containing Zr, Ag, In and Cd was observed between several rods. The experiment exhibited a multiplicity of phenomena for which the data will be invaluable for code assessment and for indicating the direction of model improvements. Example of code application with SCDAPSim is given at the end of this paper.

1. Introduction

The main goal of the QUENCH program at KIT is to investigate the core thermal response, the cladding oxidation with accompanying hydrogen release and the cooling efficiency of water injection under design basis (DBA) and beyond design basis (BDBA) accident conditions. The program was initiated in 1996 and is still on-going (Stuckert et al., 2013; Haste et al., 2015; Steinbrück et al., 2010). Experiment QUENCH-18 on air ingress and aerosol release was performed on 27 September 2017 (Stuckert et al., 2020) in the frame of the EC supported ALISA program (CORDIS Portal, 2018; Miassoedov et al., 2018). It was proposed by XJTU Xi'an (China) and supported by PSI (Switzerland) and GRS (Germany). QUENCH-18 was the worldwide first bundle experiment on air ingress including a prototypic mixed air/steam atmosphere. The primary aims were to examine the oxidation of M5® claddings in

air/steam mixture following a limited pre-oxidation in steam, and to achieve a long period of oxygen and steam starvation to promote interaction with the nitrogen. QUENCH-18 was thus a companion test to the earlier air ingress experiments, QUENCH-10 (Schanz et al., 2006) and QUENCH-16 (Stuckert and Steinbrück, 2014). In contrast to QUENCH-18, these two bundle tests were performed without steam flow during the air ingress stage. All three tests are the experimental basis for the European project QUESA on air ingress modelling (Hollands et al., 2022).

Due to air ingress as a potential risk in low probability situations of severe accidents in nuclear power plants (Powers, 2000) or accidents in spent fuel pools (Burns et al., 2014), also other research centers have performed bundle tests on air ingress with bundle geometries other than in the QUENCH facility (Stuckert et al., 2016). In addition, numerous separate-effect tests conducted at KIT and elsewhere have demonstrated

* Corresponding author at: Hermann-von-Helmholtz-Platz 1, 76344 Eggenstein-Leopoldshafen, Germany.
E-mail address: juri.stuckert@kit.edu (J. Stuckert).

the strong effect of nitrogen on the oxidation kinetics of Zr alloys (Duriez et al., 2013; Steinbrück, 2009, 2014; Steinbrück and Bottcher, 2011; Steinbrück and Schaffer, 2016; Steinbrück et al., 2017). Even very low concentrations of nitrogen (less than 1 vol%) may strongly increase reaction kinetics. The formation of porous areas with zirconium nitrides and its re-oxidation can make a significant contribution to intensive cladding oxidation during reflood.

Additionally, the QUENCH-18 experiment investigated the effects of the presence of two Ag-In-Cd control rods on early-phase bundle degradation (companion test to the QUENCH-13 experiment (Sepold et al., 2009; Lind et al., 2010)), and of two pressurized unheated rod simulators (6 MPa, He).

2. Test facility and instrumentation

The main component of the QUENCH test facility is the test section with the test bundle (Fig. 1). The facility can be operated in two modes: (a) a forced-convection mode and (b) a boil-off mode with the steam inlet line closed. QUENCH-18 was conducted in forced-convection mode, in which superheated steam from the steam generator and super-heater together with argon as a carrier and reference gas for off-gas measurements enter the test bundle at the bottom. The system pressure in the test section is usually around 0.2 MPa absolute.

Additionally to the gas inlet (steam and argon), the test section has separate inlets at the bottom to inject water for reflood (bottom quenching) and synthetic air (80% N₂ + 20% O₂) during the air ingress stage. The steam, argon and all other gases injected or produced flow from the bundle outlet at the top through a water-cooled off-gas pipe to the condenser where the steam is separated from the non-condensable gases. The water cooling circuits for bundle head and off-gas pipe are temperature-controlled to guarantee that the steam/gas temperature is high enough to avoid condensation at the test section outlet and inside the off-gas pipe and to allow quantitative measurements of steam

concentration by mass spectrometer.

The test bundle consists of 22 fuel rod simulators with a length of approximately 2.5 m and two absorber rods (Fig. 2). The fuel rod simulators are held in position by five AREVA Zr-bearing grid spacers AH 32,715 with a pitch of 12.6 mm. The rod cladding of the heated and unheated fuel rod simulators is M5® with 9.5 mm outside diameter and 0.570 mm wall thickness. Two fuel rod simulators are unheated and filled with He pressurized to 6 MPa. Twenty low-pressurized heater rods (0.23 MPa) were Kr-filled. Heating is electric by 5 mm diameter tungsten heaters of 1024 mm length installed in the rod center. The lower edge of heaters corresponds to the bundle elevation of 0 mm. The tungsten heaters are surrounded by annular ZrO₂-TZP (zirconia stabilized by yttria) pellets of 10 mm height as simulator of UO₂ pellets. At both ends of the tungsten heaters, molybdenum heaters and coppers electrodes are connected. The copper electrodes are connected by gilded slide contacts to the cables leading to the DC electrical power supply. The heating power is distributed between two groups of heated rods (10 + 10 heated rods).

There are eight corner rods installed in the bundle. Four of them, i.e. rods "A", "C", "E" and "G", are made of a Zircaloy-4 solid rod at the top and a Zircaloy-4 tube at the bottom and are used for thermocouple instrumentation. The other four rods (solid Zircaloy-4 rods of 6 mm diameter) are particularly designed to be withdrawn from the bundle to check the amount of oxidation and hydrogen uptake at specific times during the test.

The test bundle is surrounded by a 3.05 mm thick shroud of Zirconium-702 (inner diameter 82.8 mm) with a 34 mm thick ZrO₂ fiber insulation extending from the bottom to the upper end of the heated zone and a double-walled cooling jacket of Inconel (inner tube) and stainless steel (outer tube) over the entire length. The annulus between shroud and cooling jacket is purged (after several cycles of evacuation) and filled with stagnant argon at 0.22 MPa absolute. The absence of ZrO₂ insulation above the heated region and the water cooling of the bundle head are to avoid too high temperatures of the bundle in that upper bundle part.

The bundle is instrumented with 37 high-temperature (W/Re) thermocouples in the upper hot region (bundle and shroud thermocouples between elevations 650 and 1350 mm), 4 low-temperature (NiCr/Ni) thermocouples at elevations 1250 and 1350 mm (shroud), and 32 low-

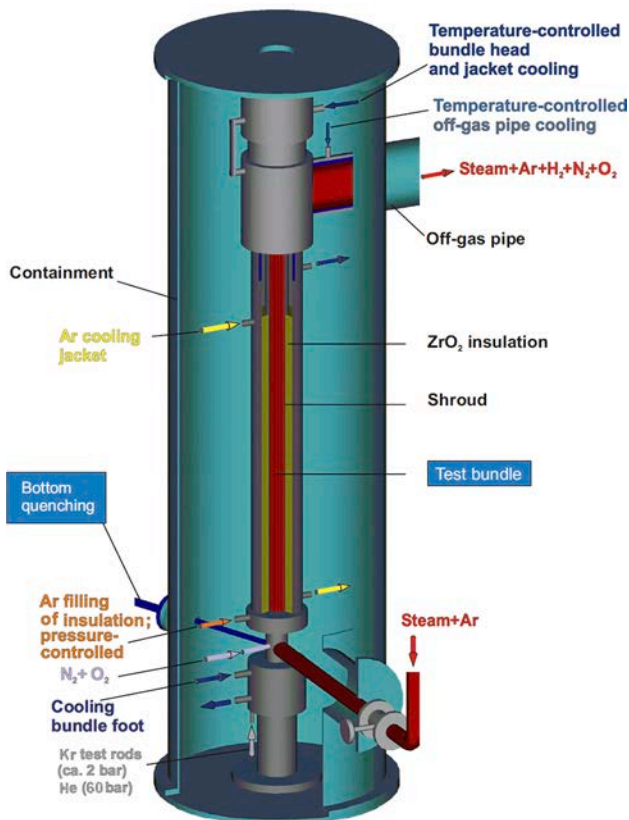


Fig. 1. QUENCH facility.

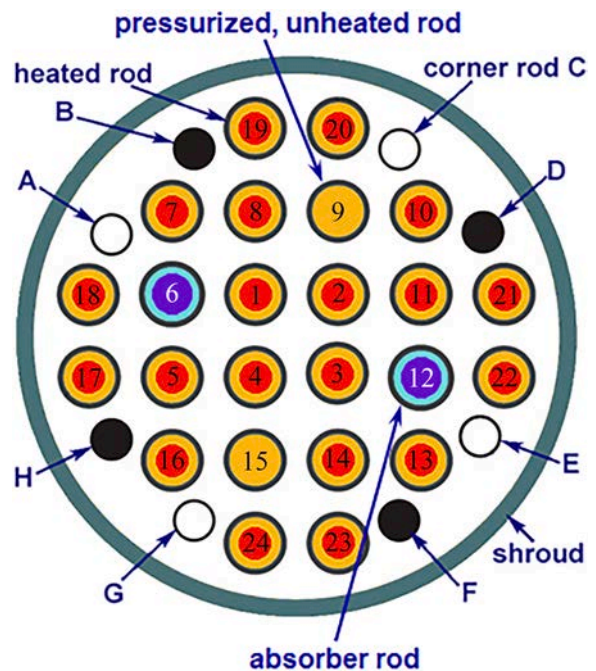


Fig. 2. QUENCH-18 bundle cross section.

temperature (NiCr/Ni) thermocouples in the lower “cold” bundle region (bundle and shroud thermocouples between 250 and 550 mm). The thermocouples attached to the outer surface of the rod cladding at elevations between 250 and 1350 mm are designated “TFS” for all heated rods (21 thermocouples). At elevations 950 and 650 mm there are two centerline high-temperature thermocouples in the central rod (designation “TCC”), which are protected from oxidizing influence of steam and air. Four other protected high-temperature thermocouples are installed at elevations 550, 650, 750, and 850 mm inside the corner rods G, E, C and A and designated “TIT”. The shroud thermocouples (designation “TSH”) are mounted at the outer surface between 250 and 1250 mm. Additionally, the test section incorporates pressure gauges, flow meters, and a water level detector.

The off-gas including Ar, He, Kr, H₂, O₂, N₂ and H₂O is analyzed by a quadrupole mass spectrometer Balzers “GAM300” whose sampling position is located at the off-gas pipe ≈2.66 m downstream the test section. The mass spectrometer allows indicating the failure of rod simulators by detection of He and Kr release.

Aerosol measurements were performed with two systems: 1) on-line device ELPI (electrical low-pressure impactor) and 2) two particle collection devices BLPI (Berners low-pressure impactor). Additionally, three polycarbonate filters (Nuclepore) were installed in parallel to the BLPI and withdrawn successively during the air ingress stage.

3. Test performance and results of online measurements

In a first transient, the bundle was heated by power increase to a peak cladding temperature of $T_{pct} \approx 1400$ K, reached at 4000 s (Fig. 3) (heat-up rate 0.3 K/s).

During this heat-up, claddings of the two pressurized rods 9 and 15 burst at temperature of ≈1035 and 1045 K, respectively (Fig. 4). These burst temperature values are lower in comparison to the values observed during the bundle test QUENCH-L2 ($T_{pct} = 1138 \pm 34$ K), which was performed with M5® claddings 10.75/0.725 mm and heat-up rate of 8 K/s (Stuckert et al., 2020), due to lower heat-up rate and thinner cladding wall.

The attainment of $T_{pct} \approx 400$ K marked the start of the pre-oxidation stage to achieve a maximum cladding oxide layer thickness of about 100 μm. The power was controlled via small variations between 8.8 and 9.4 kW, to maintain more or less constant temperatures. In line with pre-test planning calculations, about 11.5 g of hydrogen were produced in this stage, which lasted until 6310 s. At this point, the power was reduced to 3.8 kW resulting in a cooling of the bundle to $T_{pct} \approx 1080$ K,

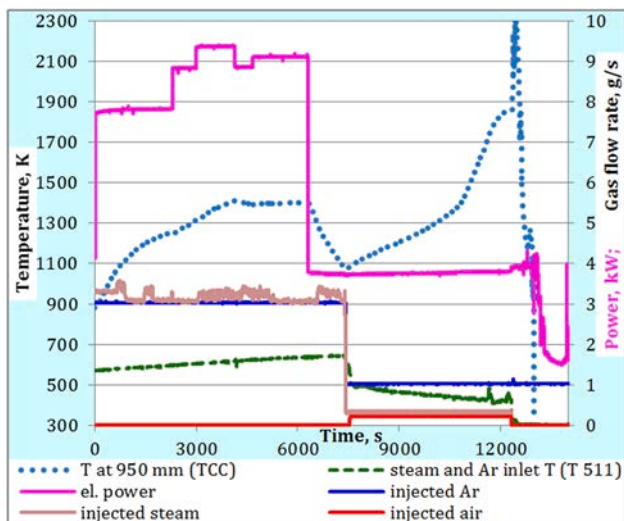


Fig. 3. Test conduct: electrical power input, selected temperatures and flow rates of injected gases.

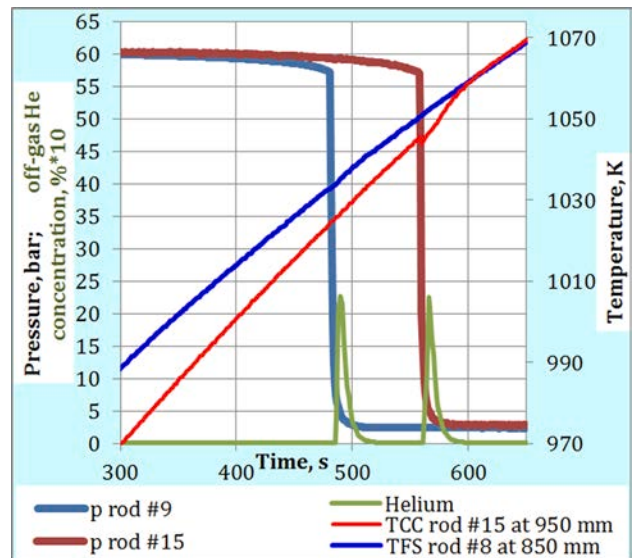
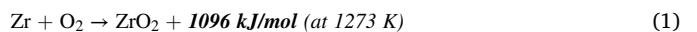


Fig. 4. Burst of pressurized rods 9 (at ≈ 850 mm) and 15 (at 950 mm).

as a preparation for the air ingress stage. The cooling stage lasted about 1100 s, until 7400 s.

Towards the end of this stage, the corner rod D was extracted from the test bundle for determination of the oxide thickness axial distribution. Metallographic measurements at the hottest (during this test stage) bundle elevation of 950 mm showed an oxide layer thickness of ≈80 μm and ≈110 μm for the α-Zr(O) layer.

In the subsequent air ingress stage, the steam flow was reduced to 0.3 g/s (7411 s), the argon flow was reduced to 1 g/s (7424 s), and air was injected at 7540 s with a flow rate of 0.2 g/s. The power was maintained at 3.8 kW to simulate a decay heat. The change in flow conditions had the immediate effect of reducing the heat transfer so that the temperatures began to rise again. After some time, measurements demonstrated a gradually increasing consumption of oxygen, starting at about 9000 s and producing noticeable chemical energy:



The failure of absorber rods with helium release and first Ag/In/Cd aerosol release was registered at 10530 s with corresponding temperature of $T_{pct} = 1350$ K (at 950 mm) and $T_{550\text{mm}} = 1300$ K (Fig. 5). The first aerosol release was dominated by Cd bearing aerosols. Later in the

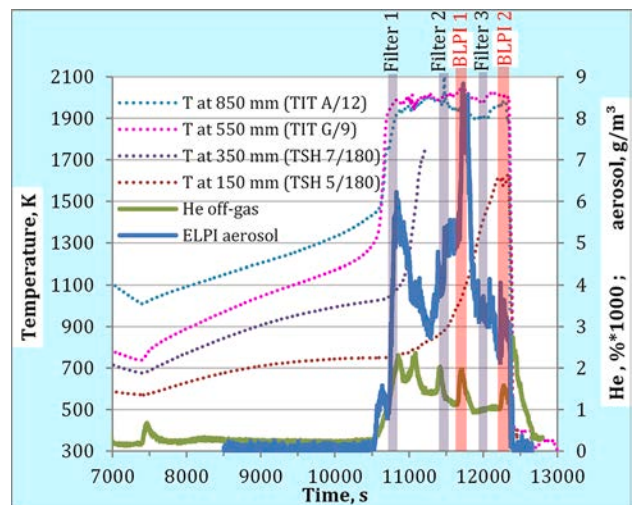


Fig. 5. Temperature escalation during air ingress and failure of absorber rods with aerosol release.

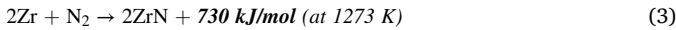
transient, a significant release of Ag was observed along with continued Cd release, as well as a small amount of In.

High aerosol concentration of several g/Nm^3 was measured until the isolation of the aerosol measurement system at the time of the quench initiation. Effective diameter of sampled particles (ELPI and BLPI) was measured to be between 0.4 and $10\ \mu\text{m}$ (main part of released particles had diameter of about $1\ \mu\text{m}$). Based on the EDX analysis, a rough estimation of absorber material releases during the whole test was performed (Table 1) (Kalilainen et al., 2019).

In contrast to the QUENCH-16 test (performed with the air ingress stage without steam flow), oxidation of bundle parts in steam caused release of hydrogen and additional chemical energy (power about 4 kW) and consequently more intensive acceleration of bundle heat-up:



A strong temperature escalation started at about 10590 s at the bundle elevation of 550 mm and propagated to the upper and lower elevations between 150 and 850 mm (Fig. 5). A period of oxygen starvation started at about 10700 s and was followed (about 300 s later) by almost complete steam consumption. Shortly before that time (10640 s), partial consumption of the nitrogen was first observed, indicating local oxygen and steam starvation which promoted the onset of nitriding of claddings, shroud, corner rods and absorber guide tubes:



Following this, the temperatures continued to increase and stabilized at melting temperature of Zr bearing materials until water injection was initiated at 12330 s. The escalation stopped at the melting point due to the relatively low heat input ($\approx 12\ \text{kW}$ consisting of $\approx 4\ \text{kW}$ electric heat and two chemical heat sources each $\approx 4\ \text{kW}$ due to the oxidation of zirconium in steam and air), as well as the high specific heat of fusion of zirconium ($h_{\text{fus}} = 185.7\ \text{kJ/kg}$) in comparison with its specific heat at the stage of temperature escalation ($c \approx 0.27\ \text{kJ/kg/K}$). According to crucible experiments, a noticeable dissolution of zirconium oxide by metallic zirconium begins only from 2300 K (Hofmann et al., 1999); therefore, the cladding melt appearing at $\approx 2000\ \text{K}$ remains localized between the outer oxide layer and the pellet. This is also confirmed by the localization of the melt under the outer oxide layer in the previous QUENCH experiments (Stuckert et al., 2010, Stuckert et al., 2011).

Thus there was a period of 1630 s of strong steam and complete oxygen consumptions and hence starvation in at least part of the bundle (Fig. 6). The total consumption of oxygen, steam and nitrogen were 100 ± 3 , 450 ± 10 and $120 \pm 3\ \text{g}$, respectively. During this starvation period, a noticeable production (about 25 mg/s, totally $45 \pm 1\ \text{g}$) of hydrogen was measured.

Toward reaching of the cladding melting point, a lower part of the second corner rod (below elevation 550 mm) was removed (11014 s). Metallographic analysis of the cross section of this rod at 520 mm shows $\alpha\text{-Zr(O)}$ and ZrN layers at the boundaries of the oxide layer (Fig. 7). Spalling of ZrO_2 scales was observed.

Significant release of Kr beginning at 10730 s and continued until quench initiation indicated failures of fuel rod simulators, probably mostly due to crack development in the intensively growing oxide layer. The shroud failure with penetration of additional argon flow into the bundle was registered at 11253 s.

The reflood was initiated simultaneously with turning off the air and steam flows, switching the argon injection to the top of the bundle,

Table 1
Release of Cd, In, and Ag.

Element	Released, g	Fraction from total, %
Cadmium	9.0	14.3
Indium	1.2	0.7
Silver	6.6	0.6
Total	16.8	1.3

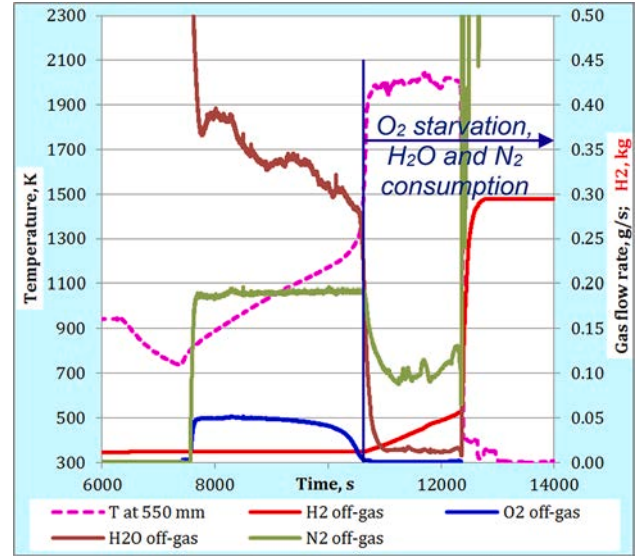


Fig. 6. Outlet gas behavior: consumption of O_2 , H_2O and N_2 during air ingress; release of H_2 during air ingress and reflood.

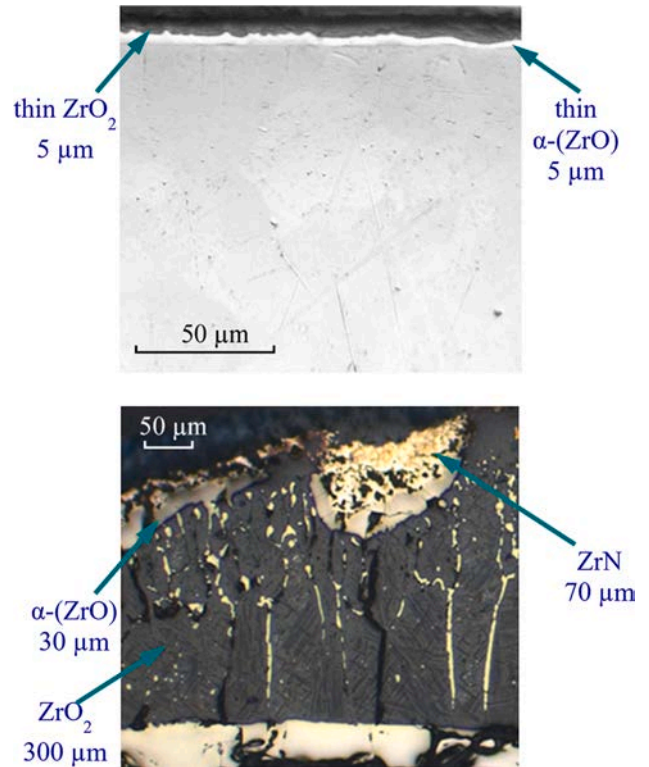
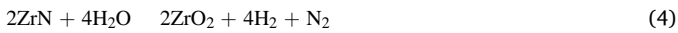


Fig. 7. Comparison of corner rod structures at elevation of about 520 μm for rod D withdrawn at the air ingress initiation (top) and rod H withdrawn at the end of temperature escalation (bottom).

followed by fast filling the lower plenum of the test section with 4 kg of water, and continuing by injecting 50 g/s of water. The power remained at 3.8 kW during the reflood.

Due to strong exothermic reaction with metal melt in the bundle middle and claddings at upper elevations not protected by oxide layer (dissolved during starvation stage (Stuckert and Veshchunov, 2008)), almost immediately after the start of reflood there was a temperature excursion above the middle of the bundle. The direct interaction of the melt with the steam leads to an even more accelerated heating of the

bundle, since the rate of the steam-zirconium reaction with the melt is almost three times higher than its rate when interacting with metal claddings in the solid state (Stuckert et al., 2019). About 30 MJ chemical energy were released during 150 s. This escalation led to maximum measured temperatures of about 2430 K (Fig. 8). Cooling was established at the middle bundle elevation (550 mm) ca. 70 s after the start of injection, but was delayed further at upper elevations. Reflood progressed rather slowly, first due to filling of the space between shroud and cooling jacket and after that due to partial bundle melting. The TFS thermocouples on the cladding surface were wetted with a two-phase liquid when the water front was 300–500 mm below the wetting elevation. Final quench was achieved after about 800 s. A significant quantity of hydrogen was generated during the reflood (238 ± 2 g) (Fig. 6). Nitrogen release (>54 g) due to re-oxidation of nitrides was also registered:



4. Post-test bundle examinations

The overview of the bundle top shows strong cladding oxidation. Absorber melt relocation to the bundle bottom was observed by video-scope inspection at the position of withdrawn corner rods. According to thermocouple measurements, the first absorber melt relocation from elevations above 550 mm to lower elevations was registered at 10680 s, shortly before failure of heated rods.

The facility was disassembled for post-test examinations. Due to extreme brittleness, the bundle broke into two parts at the elevation of about 1100 mm (Fig. 9). It was practically not possible to separate the shroud and the ZrO_2 heat insulation between elevations 200 and 550 mm due to partial shroud melting. Frozen melt rivulets were recognized at the oxidized cladding surface at elevations above 550 mm.

The bundle was embedded in epoxy resin, which was solidified after two weeks. Then it was cut into slices with a diamond saw. The metallographic investigations of claddings at upper elevations between 1300 and 1350 mm shows strong but not complete oxidation for peripheral bundle rods and relocation of metallic melt from inner rods (Fig. 10). The melt was formed here during the temperature escalation after initiation of reflood.

The metallographic investigations of the bundle cross section at the



Fig. 9. Post-test appearance of bundle at the angle view of 0°.

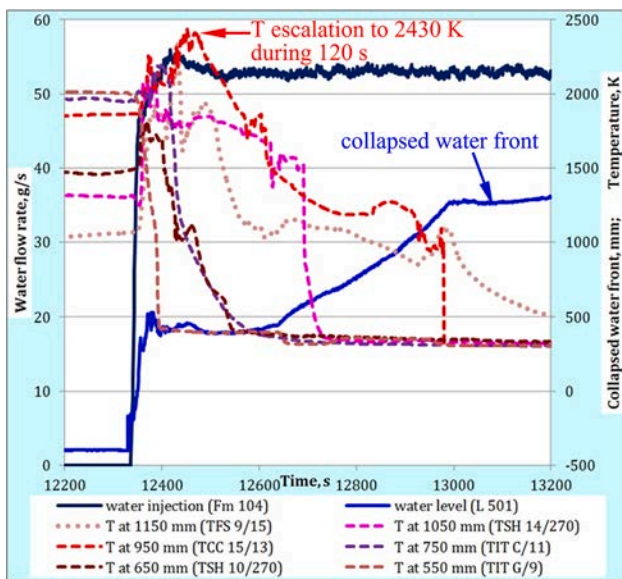


Fig. 8. Progress of collapsed water front and temperatures during the reflood stage.

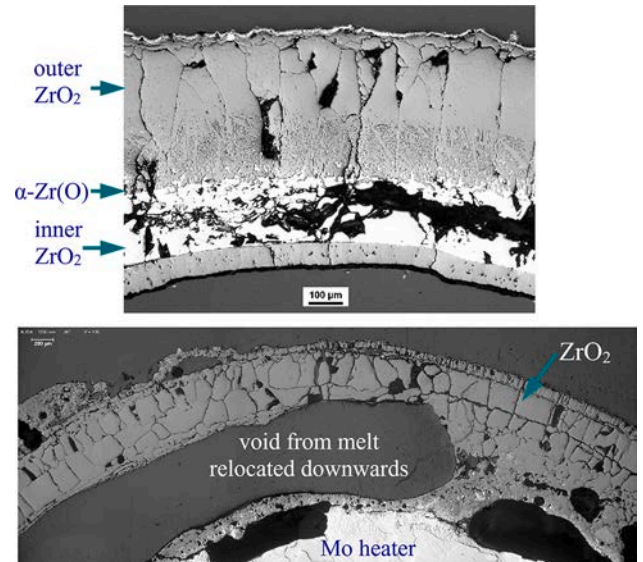


Fig. 10. Cladding structures of outer (top) and internal (bottom) rods at upper bundle elevations above 1300 mm.

hottest elevation 950 mm showed completely oxidized parts of claddings and remaining melt formed here during reflood. Several pellets were partially dissolved at this elevation by molten Zr. The bulk of frozen pools is very porous and the area of pool cross section is strongly

limited without noticeable blockage of the bundle cross section. A detailed study of cladding oxide scales shows the presence of porous clusters inside them, which should correspond to the locations of *nitrides* re-oxidized during reflood (Fig. 11).

One part of the melt formed at elevations above 900 mm was relocated downwards and was frozen at lower bundle elevations together with the melt formed there (Fig. 12). The formation of a melt at lower elevations between 350 and 850 mm occurred already in the air ingress stage, since the temperature here sharply escalated and remained at the level of the cladding melting point for a long period lasting more than 1000 s (temperature profile here is similar to the thermocouple reading in Fig. 6).

For the elevation 750 mm, a relatively large oxidized molten pool was formed at the position of the previously downward relocated absorber rod 12 (Fig. 13). Similar to other bundle elevations, the bulk of the frozen pool is very porous. The voids were presumably formed as parts of gas channels during steam flow. Unlike 950 mm, small metal pools containing Zr and Fe can be observed at this elevation. It should be the frozen parts of steel absorber cladding. Other metal pools were formed by droplets of Mo relocated from bundle top. Additionally, small zones of zirconium nitrides were observed. One of two unheated rods was completely destroyed (rod 9) and the pellets of this rod absent between 750 and 950 mm. The bundle blockage by relocated melt was about 10%; it was the maximum blockage for the bundle axial positions without grid spacers.

Significant part of the melt was collected inside the third grid spacer between 550 and 590 mm (Fig. 14). The bundle blockage reached here 30%, which is the maximum value for the entire assembly. Due to very high temperatures at this elevation (Fig. 5), the melt was mostly oxidized. However, there are “pools” with partially oxidized melt with ceramic precipitates inside.

Fig. 15 shows surroundings of rod 2 at elevation 560 mm with completely and partially oxidized melt regions. Additionally, two positions at the pellet boundary have a porous structure, which is typical for nitriding of α -Zr(O) during steam and oxygen starvation with the following re-oxidation during the flooding. The corresponding structure with re-oxidized nitrides is shown in Fig. 16. Re-oxidized separate nitrides were also found in other areas: inside not completely dissolved segments of oxidized cladding of rod 14 and in the surroundings of

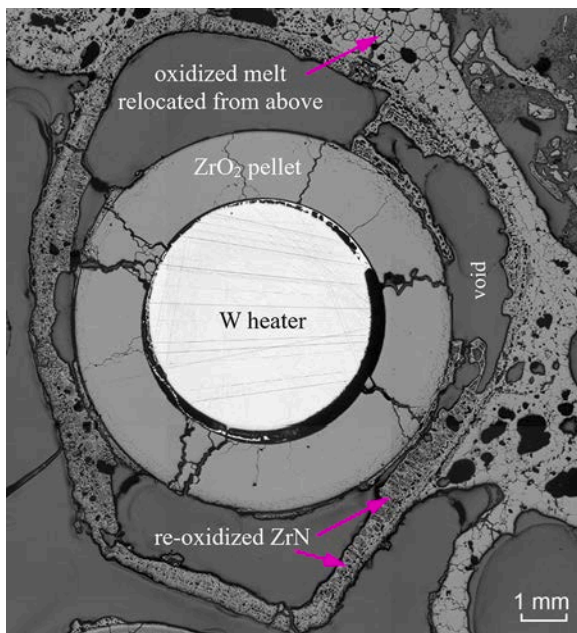


Fig. 11. Oxidized cladding of rod 4 at 950 mm with re-oxidized nitrides and surrounded by frozen melt.

downwards relocated absorber rod 12.

In place of the absorber rod 12, parts of its stainless steel cladding and M5 guide tube that formed a eutectic melt were found.

For the elevation 350 mm, molten particles of absorber rod 12 penetrated through the failed cladding of rod 2, mixed with molten cladding metal and froze in the gap between cladding oxide and pellet (Fig. 17).

As a result of steam and oxygen starvation stages (with formation of α -Zr(O) layer at the ZrO_2 surface (Stuckert and Veshchunov, 2008)) and simultaneous nitrogen ingress, *nitrides* were formed inside cladding oxides (reaction of N_2 with α -Zr(O) (Steinbrück, 2014)). These nitrides were re-oxidized during the following reflood stage (Fig. 18). The re-oxidized porous structure is similar to the structure of “nitride pockets” formed in strongly oxidized claddings of the QUENCH-10 bundle (Schanz et al., 2006).

For the elevation 160 mm, the temperature at the outer cladding and shroud surfaces did not reach the melting point of Zr alloy neither during the temperature escalation in the air ingress stage, nor during the following reflood stage. Partially oxidized Zr-O melt blocked only small part of the bundle. The oxidation of the molten pool occurred not only along its periphery, but also in the bulk (Fig. 19). Numerous ZrO_2 precipitates show that the pool oxidation took place not only during cooling, but also at continuous high temperatures (Veshchunov et al., 2002).

According to REM/EDX analysis, traces of yttrium inside melt indicate relocation of dissolved parts of pellets. 160 mm is the lowest elevation with relocated pellet material.

Both absorber rods are absent also at this elevation. Parts of molten materials of absorber rods were not only mixed with metal melt relocated from above, but also penetrated into the gap between claddings of fuel rod simulators and pellets. In some cases, Ag and In penetrated even into the outer regions of pellets to a depth up to 150 μm .

For the bundle elevation 65 mm, the maximum temperature reached during escalation was 1010 K. The claddings, shroud and corner rods are only slightly oxidized. There is a partial blockage of the bundle by (Ag, In, Cd) and Zr-bearing melt formed from parts of absorber rods and relocated from above (Fig. 20). Two types of frozen metal pools were formed: pure (Ag, In) and Zr based melt (mixed with Ag, In). The total area of blockage the gas channel by the relocated melt was about 23%.

The maximum temperatures registered at the elevation 40 mm were about 700 K and claddings practically did not oxidize. Only materials of absorber rods (including materials of stainless steel absorber cladding and Zr-bearing guide tube) were registered here inside the molten pools outside rods (Fig. 21). Precipitation of intermetallic phases $AgZr$, $InZr_2$, and Zr_3Fe inside the (Ag, In, Cd) melt relocated from above was observed. Similar to 60 mm, the gas channel blockage by the relocated melt was 23%. Some droplets and rivulets of absorber melt have relocated to the bundle bottom (475 mm).

5. Post-test modelling with SCDAPSim

Modelling was performed with SCDAPSim/Mod3.5 (Allison and Hohorst, 2010) which comprises a two-fluid treatment of the thermal-hydraulics and semi-mechanistic modelling of the core degradation from its onset through to the late phase molten pool behavior. Comparisons between the experimental results and the simulations are extensively discussed (Birchley et al., 2019) for a variety of modelling assumptions regarding oxidation kinetics and the (at the time) uncertain state of the bundle during reflood.

Here we confine attention to just two aspects of the simulation, (i) the consumption of oxygen and restart of hydrogen release during the air stage, and (ii) the oxidation during reflood.

The modelling includes ballooning and burst of pressurized rods, control rod failure due to material interactions between cladding and guide tube, cladding oxidation, and fuel rod degradation. The SCDAP-Sim default oxidation model is the pairing Cathcart-Pawel (CP) (Pawel et al., 1979) and Urbanic-Heidrick (UH) (Urbanic and Heidrick, 1978)



Fig. 12. Cladding oxidation and distribution of cladding and absorber melts between bundle elevations 65 and 950 mm.

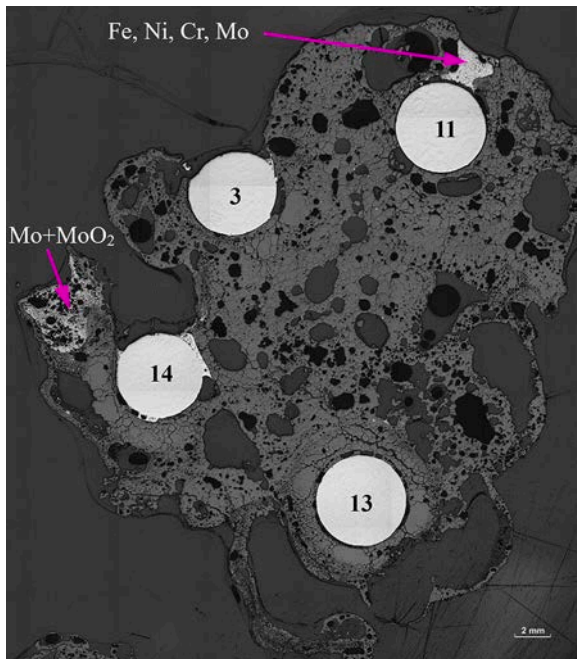


Fig. 13. Completely oxidized porous molten pool formed in the place of vanished absorber rod 12 at 750 mm.

correlations for oxidation in the temperature regimes below 1853 K (low/intermediate) and above 1873 K (high), with linear interpolation in between. The present code version allows additional options, including the Leistikow-Schanz (LS)/Prater-Courtright (PC) (Schanz et al., 2004) pair of correlations for the lower and high temperatures, respectively, which was used to examine sensitivity to steam oxidation kinetics. The Uetsuka-Hofman correlation (Uetsuka and Hofmann,

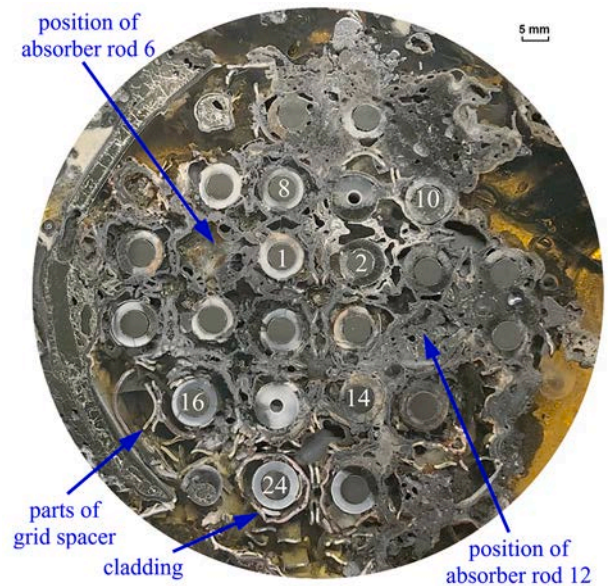


Fig. 14. Bundle cross section 560 mm, top view: mostly oxidized melt, frozen inside the grid spacer.

1985) was used for the oxygen oxidation rate. All these correlations assumed parabolic kinetics of cladding oxidation. It is assumed that steam is not consumed in the local presence of oxygen. Accelerated oxidation in air is modelled in a similar way to breakaway in steam (or oxygen), i.e. a transition from parabolic to linear kinetics is triggered when the oxide layer reaches a critical thickness, δ_{crit} . It is applied in the presence of nitrogen with either (or both) oxygen and steam, and the post-transition state persists even after the end of the air stage. Different parameter values for δ_{crit} are used with and without nitrogen present.

The input model is based on the one used in analyses of the previous

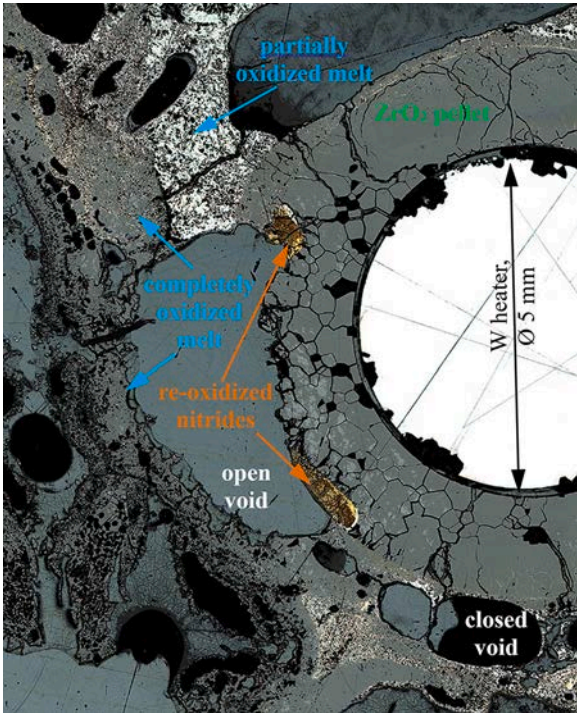


Fig. 15. Surroundings of rod 2 at elevation 560 mm.

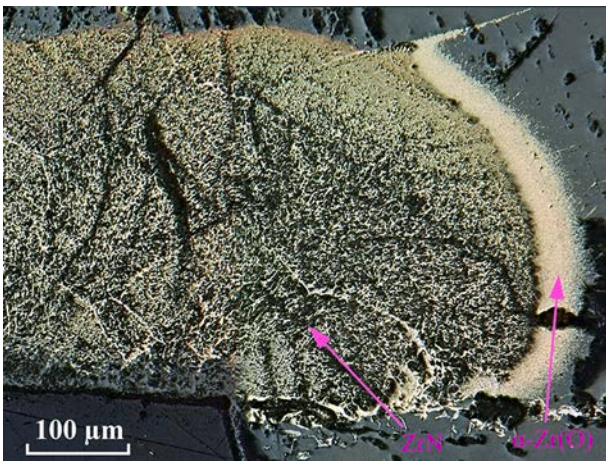


Fig. 16. Partially re-oxidized zirconium nitrides at elevation 560 mm.

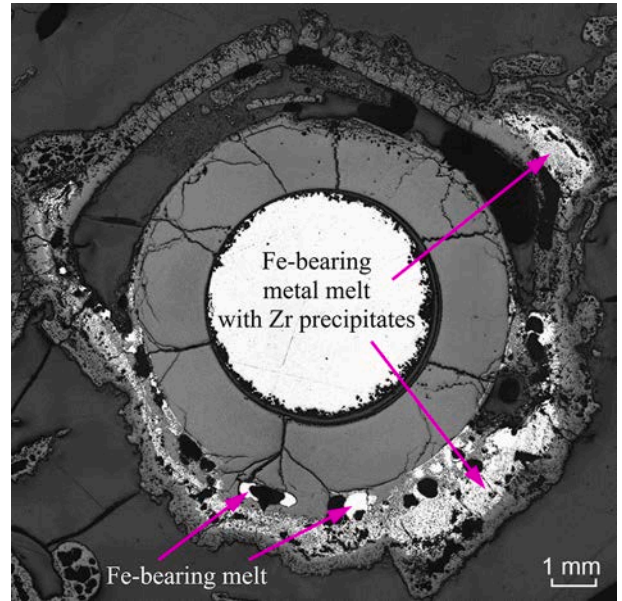


Fig. 17. Penetration of molten absorber cladding materials under cladding oxide of rod 2 at elevation 350 mm.

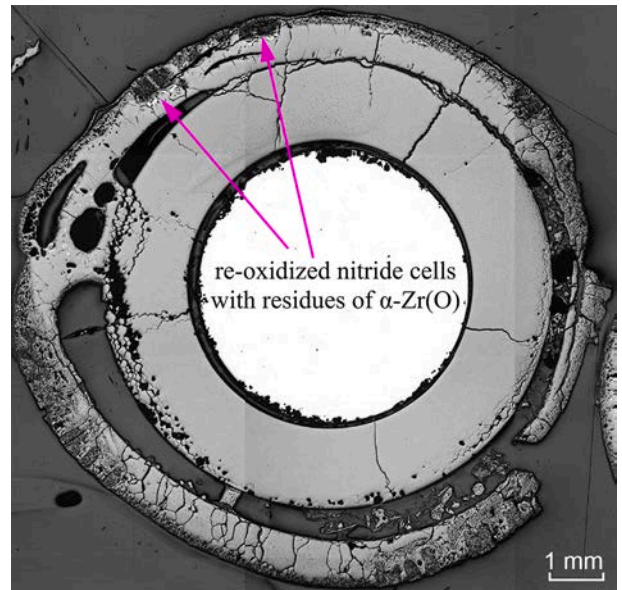


Fig. 18. Re-oxidized nitride cells formed inside thick cladding oxide of rod 23 at elevation 350 mm.

QUENCH experiments, starting with QUENCH-06 (Sepold et al., 2004), which was subject of CSNI International Standard Problem 45 (Hering et al., 2002). The present model was evolved directly from the model used to analyze the QUENCH-16 test (Fernandez-Moguel and Birchley, 2013) to reflect the change in bundle configuration and the inclusion of the two absorber and two unheated pressurized rods.

Experimental programs on reflood from high temperature have shown that the injection of coolant does not always lead to immediate cooling. In some cases there was a significant temperature excursion, as a result of rapid oxidation of the cladding, e.g. QUENCH-02, -03 (Hofmann et al., 2000), -07, -09 (Sepold et al., 2006), and -16 (Stuckert and Steinbrück, 2014). A strong excursion was typically observed if degradation had already started or if the oxide layer had been weakened following oxidant starvation, causing un-oxidized metallic material to be exposed to the steam flow. The melt oxidation is very intensive and is a significant driver for the hydrogen release (Veshchunov et al., 2002). SCDAPSim includes a simple phenomenological model for rapid

oxidation of molten metallic that is released following a breach of the oxide layer. An oxide layer forms on the molten metallic but is breached again, so the un-oxidized surface may be repeatedly renewed. The occurrence of breach of the oxide layer is essentially determined by a user-specified temperature criterion, which can take any value in the interval from 2200 K which is somewhat above the metallic melting temperature, to 2600 K which is somewhat below the oxide melting temperature. The default criterion is 2500 K.

Calculation of the air-ingress stage shows a clean switch from complete oxygen consumption to hydrogen release with no period of overlap (Fig. 22) (Birchley et al., 2019). This calculated behavior is implied by the single channel input model in conjunction with the code model exclusion of oxygen and steam being consumed simultaneously and locally. By contrast, the experiment shows a minor overlap, possibly due to variations in oxygen concentration across the bundle. Although any

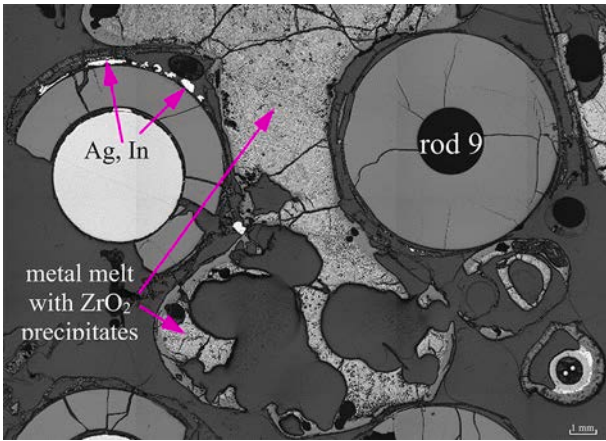


Fig. 19. Melt between rods 8 and 9 at elevation 160 mm, penetration of absorber materials in the gap between pellet and cladding.

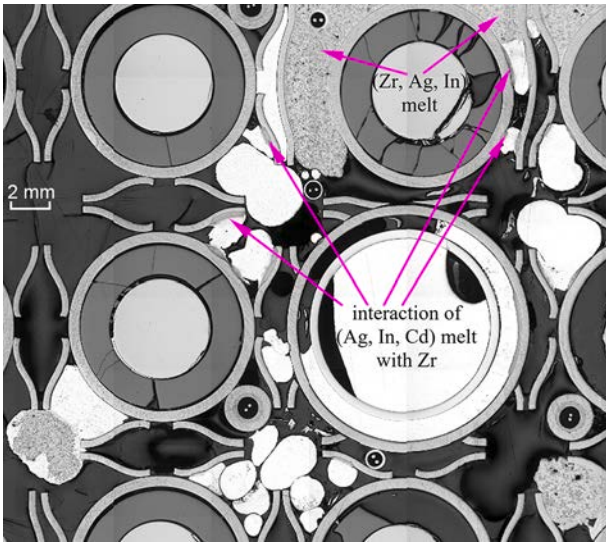


Fig. 20. Molten pools at elevation 65 mm formed around absorber rod 12 from absorber material relocated from upper bundle elevations.

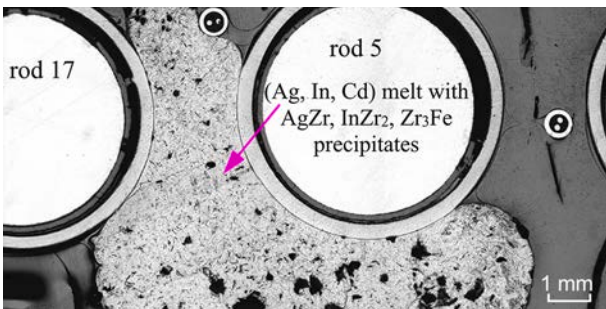


Fig. 21. Absorber melt frozen at -40 mm.

hydrogen thus produced would be expected to recombine with residual oxygen, the flow might not have been sufficiently mixed for that to have happened when the starvation at the top of the bundle was still local to the hotter locations. The measured temperatures, 400 – 600 K, between the bundle and spectrometer location were too low for hydrogen-oxygen recombination.

The data also show uptake of between 0.05 and 0.1 g/s nitrogen starting very shortly before the onset of steam starvation (Fig. 6). It

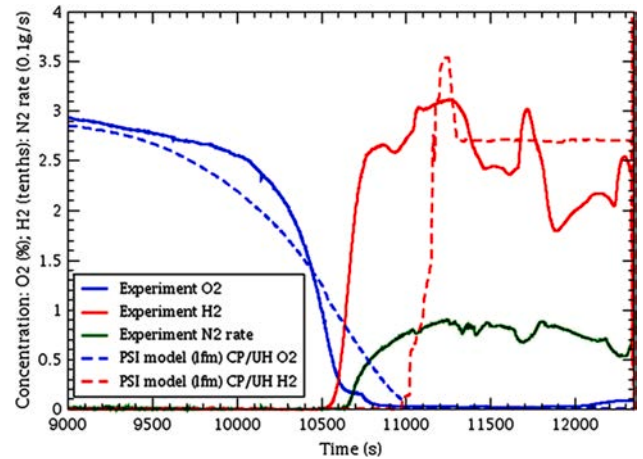


Fig. 22. Comparison for calculated and experimental H₂ and O₂ concentrations at bundle exit during air ingress (also experimental N₂ flow rate is shown).

would seem that the uptake is prevented by the presence of steam, and that the small overlap in timing might be due to local starvation. The uptake begins before complete steam starvation but does not reach its maximum value until all the steam is consumed. However, it is not clear if the presence of steam and nitrogen uptake affect each other's reaction with the cladding. It may be that the uptake increased together with the extent of the oxygen-starved region. The used version of SCDAPSim does not contain any model for Zr-nitrogen reactions, a serious limitation in current versions.

The strong escalation observed during reflow was not captured using the default options for oxidation kinetics (CP-UH) and criterion for cladding oxide breach (2500 K). Use of the Ls-PC correlation coupled with reduction of the breach criterion to 2200 K enabled a significant improvement, due to the faster kinetics of the PC correlation and the exposure of metallic melt to the flowing steam. The large early release of hydrogen was still underestimated as the calculated steam flow was insufficient to support the observed excursion. Although not predicted in the simulations, examinations revealed noticeable relocation of material of absorber rods, including the M5 guide tube and steel cladding) to the lower part of the test section, 475 to +60 mm, which partially blocked the gas channel and could promote strong steam generation during early part of reflow. In a further sensitivity an additional (1800 g) steam flow was postulated during the first two minutes of reflow. Results of the hydrogen release in the various calculations are compared with the experiment in Fig. 23.

The release and relocation of molten claddings following breaches of

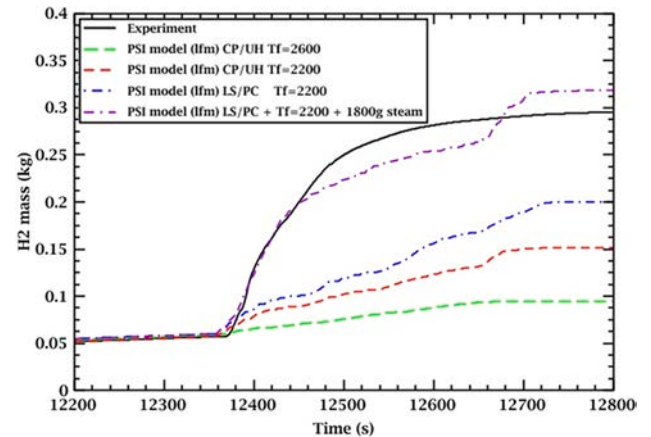


Fig. 23. Comparison for calculated and experimental H₂ generation using alternative models and assumptions.

the oxide scales resulted in numerous thermocouple failures and modified the temperature profiles. A significant quantity of nitride was formed during the period of oxygen and steam starvation which, together with the molten cladding, was very likely to have made the bundle conducive to rapid oxidation during reflood. Breach of the shroud and consequent ingress of water are also likely to have impacted the oxidation excursion. All of these factors are problematic from both a modelling and experimental point of view. QUENCH-18 is therefore particularly relevant to recent and current efforts to address nitriding issues (Hollands et al., 2022; Jackel et al., 2019; Park, 2020).

6. Summary and conclusions

QUENCH-18 was the first large-scale bundle test including a prototypical experiment stage in air + steam mixture. The bundle contained 20 electrically heated and 2 unheated rods with M5® cladding as well as 2 Ag-In-Cd absorber rods. The test was performed at KIT on September 27, 2017 in the framework of the EC-China ALISA project. Three typical features of QUENCH-18 were: moderate pre-oxidation to $\approx 80 \mu\text{m}$ of oxide layer (less than in the reference test QUENCH-16), a long period of oxygen starvation during the air and steam ingress stage (1770 s instead 800 s for the QUENCH-16 test performed without steam injection during air ingress), and reflood initiation at the melting point of the cladding ($\approx 2000 \text{ K}$ instead of 1700 K for QUENCH-16).

The claddings of unheated and pressurized rods burst at 1045 K at a heat-up rate of 0.3 K/s . These burst temperature is lower in comparison to burst temperatures observed during the bundle test QUENCH-L2 ($T_{\text{pct}} = 1138 \pm 34 \text{ K}$) due to lower heat-up rate and thinner cladding wall.

The temperature escalation during the air ingress between elevations 150 and 850 mm was significantly stronger than for QUENCH-16 mainly due to additional exothermal cladding oxidation in steam (corresponding additional chemical energy of $\approx 4 \text{ kW}$ was even slightly higher than electrical power). The metallographic investigations of the Zry corner rod, withdrawn at the end of escalation, showed formation of ZrN inside α -(ZrO) layer formed on the oxide layer during oxygen and steam starvation.

Releases of aerosols and helium were registered at the beginning of temperature escalation (failure of absorber rods). Simultaneously, the readings of cladding surface thermocouples below elevation of 550 mm indicated the relocation of absorber melt.

During the starvation period about 100 and 450 g oxygen and steam were consumed. During the steam consumption period about 45 g hydrogen were released. In the same time, a partial consumption of nitrogen (about 120 g) was registered. Formation of zirconium nitrides was observed in the bundle middle part (elevations above 500 mm).

Due to the relatively low heat input ($\approx 3 \cdot 4 \text{ kW} = 12 \text{ kW}$ as a result of electrical heating and exothermal reactions with steam and air), as well as the high specific heat of fusion of zirconium in comparison with its specific heat at the stage of temperature escalation, the escalation stopped when the melting point was reached. The cladding melt appearing at $\approx 2000 \text{ K}$ remains localized between the outer oxide layer and the pellet.

Initiation of reflood with 50 g/s water caused strong temperature escalation to about 2430 K at elevations between 750 and 1150 mm resulting in about 238 g hydrogen release. It is significantly more than for QUENCH-16 (128 g) performed also under air ingress conditions, but with the formation of a smaller amount of melt. The bundle temperatures at reflood initiation were much higher than in QUENCH-16. During re-oxidation of zirconium nitrides more than 54 g nitrogen and 15 g hydrogen were released. The rest and the largest part of the released hydrogen should be associated with the oxidation of the claddings in the upper part of the bundle and the oxidation of the metal melt in the middle part of the bundle. Final cooling was achieved after about 800 s , which is noticeably longer than in most previous QUENCH tests where cooling occurred in $300\text{--}400 \text{ s}$.

The metallographic investigations of the bundle show strong cladding oxidation and Zr melt formation below the elevation of 1430 mm . The Zr melt was completely oxidized above 350 mm and caused a bundle blockage at several elevations with a maximum value of 30% inside the grid spacer at 560 mm . No downwards relocated pellet material was registered below 160 mm . No cladding melt was relocated below 65 mm . The absorber melt was collected at elevations between 40 and 350 mm , but partially relocated down to the bundle foot, and consisted of intermetallics containing Zr, which precipitated inside the solidified mass of the (Ag, In, Cd) absorber. The bundle blockage by relocated absorber materials at the elevations between the bundle bottom (475 mm) and second grid spacer ($+65 \text{ mm}$) reached a maximum of 23% .

The modelling with SCDAPSim gives generally good agreement for the pre-reflood test stage, in particular the oxidation by steam and oxygen. However, modelling of the reflood remains problematic. The lack of models for nitride formation and oxidation limit the capability to capture the reflood excursion.

CRedit authorship contribution statement

Juri Stuckert: Conceptualization, Methodology, Formal analysis, Investigation, Data curation, Writing - original draft, Writing - review & editing, Visualization, Supervision. **Martin Steinbrueck:** Conceptualization, Methodology, Investigation, Data curation, Writing - review & editing. **Jarmo Kalilainen:** Methodology, Formal analysis, Investigation, Writing - review & editing. **Terttaliisa Lind:** Methodology, Formal analysis, Investigation, Writing - review & editing. **Jonathan Birchley:** Methodology, Software, Formal analysis, Investigation, Writing - original draft, Writing - review & editing.

Declaration of Competing Interest

The authors declare that they have no known competing financial interests or personal relationships that could have appeared to influence the work reported in this paper.

Acknowledgements

The authors gratefully acknowledge funding by Euratom to support the work within the ALISA project under the Grant Agreement 295421. The bundle materials were provided by AREVA.

The authors thank Mr. Moch and Ms. Peters for the extensive bundle preparation and Ms. Stegmaier for the detailed SEM/EDX analysis.

References

- Allison, C. M., Hohorst, J. K., 2010. Role of RELAP/SCDAPSIM in Nuclear Safety. Science and Technology of Nuclear Installations, vol. 2010, article ID 425658, doi:10.1155/2010/425658.
- Birchley, Jonathan C., Stuckert, J., Steinbrueck, M., Grosse, M., 2019. Preliminary interpretative analysis of the QUENCH-18 bundle test using SCDAPSim/mod3.5. Ann. Nucl. Energy 130, 20–33. <https://doi.org/10.1016/j.anucene.2019.02.022>.
- Burns, E.T., Lee, L.K., Duvall, A.H., 2014. Spent Fuel Pool Risk Assessment Integration Framework and Pilot Plant Application, Report EPRI 3002002691, <https://www.epri.com/research/products/3002002691>.
- CORDIS Portal, 2018. Results of the ALISA project. Final Report Summary. <https://cordis.europa.eu/project/id/295421/reporting>.
- Duriez, C., Drouan, D., Pouzadoux, G., 2013. Reaction in air and in nitrogen of pre-oxidised Zircaloy-4 and M5™ claddings. J. Nucl. Mater. 441 (1-3), 84–95. <https://doi.org/10.1016/j.jnucmat.2013.04.095>.
- Fernandez-Moguel, Leticia, Birchley, Jonathan, 2013. Analysis of QUENCH-10 and -16 air ingress experiments with SCDAPSim3.5. Ann. Nucl. Energy 53, 202–212. <https://doi.org/10.1016/j.anucene.2012.08.030>.
- Haste, T., Steinbrück, M., Barrachin, M., de Luze, O., Grosse, M., Stuckert, J., 2015. A comparison of core degradation phenomena in the CORA, QUENCH, Phébus SFD and Phébus FP experiments. Nucl. Eng. Des. 283, 8–20. <https://doi.org/10.1016/j.nucengdes.2014.06.035>.
- Hering, W., Homann, Ch., Lamy, J.-S., Miassoedov, A., Schanz, G., Sepold, L., Steinbrück, M., 2002. Comparison and interpretation report of the OECD international standard problem no.45 exercise (QUENCH-06). Scientific report FZKA-6722, Karlsruhe. doi: 10.5445/IR/270052469.

- Hofmann, P., Homann, C., Leiling, W., Miassoedov, A., Piel, D., Schanz, G., Schmidt, L., Sepold, L., Steinbrück, M., 2000. Experimental and calculational results of the experiments QUENCH-02 and QUENCH-03. Scientific report FZKA-6295, Karlsruhe, doi:10.5445/IR/270048148.
- Hofmann, P., Stuckert, J., Miassoedov, A., Veshchunov, M.S., Berdyshev, A.V., Boldyrev, A.V., 1999. ZrO₂ dissolution by molten Zircaloy and cladding oxide shell failure. New experimental results and modelling. Scientific report FZKA-6383, Karlsruhe. <https://doi.org/10.5445/IR/270046616>.
- Hollands, T., Beuzet, E., Vasiliev, A., Kaliatka, T., Birchley, J., Kostka, P., Steinbrück, M., Stuckert, J., Hózer, Z., 2022. Status of benchmark exercises in the frame of the NUGENIA QUESA project. in: Proceedings of 19th International Topical Meeting on Nuclear Reactor Thermal Hydraulics (NURETH-19), Brussels, 2022., ttp.
- Jackel, B. S., Terttaliisa Lind, Leticia Fernandez-Moguel, Martin Steinbrück, Sanggil Park, 2019. Application of a newly developed computer code model for nitriding and re-oxidation of cladding materials on separate effect tests and integral experiments. in: Proceedings of 9th European Review Meeting on Severe Accident Research (ERMSAR 2019), Prague, March 18-20, 2019, paper 024, https://www.ermarsar2019.com/upload/wwt/31_ERMSAR-2019-PROCEEDINGS.pdf.
- Kalilainen, J., Lind, T., Stuckert, J., Bergfeldt, T., Sippula, O., Jokiniemi, J., 2019. The measurement of Ag/In/Cd release under air-ingress conditions in the QUENCH-18 bundle test. *J. Nucl. Mater.* 517, 315–327. <https://doi.org/10.1016/j.jnucmat.2019.02.021>.
- Lind, T., Csordás, A.P., Nagy, I., Stuckert, J., 2010. Aerosol behavior during SIC control rod failure in QUENCH-13 test. *J. Nucl. Mater.* 397 (1-3), 92–100. <https://doi.org/10.1016/j.jnucmat.2009.12.013>.
- Miassoedov, A., Gaus-Liu, X., Liao, Y., Chen, P., 2018. ALISA project: Access to large infrastructures for severe accidents in Europe and China. Proceedings of 12th International Topical Meeting on Reactor Thermal-Hydraulics, Operation, and Safety (NUTHOS 2018), Qingdao, China., 14.10.2018 – 18.10.2018, paper 911.
- Park, Sanggil, 2020. Nitriding and Re-oxidation Behavior of Zircaloy-4 at High Temperatures. Doctoral Thesis. ETH Zürich. doi:10.3929/ethz-b-000459694.
- Pawel, R.E., Cathcart, J.V., McKee, R.A., 1979. The kinetics of oxidation of zircaloy-4 in steam at high temperatures. *J. Electrochem. Soc.* 126 (7), 1105–1111. <https://doi.org/10.1149/1.2129227>.
- D.A. Powers, Technical issues associated with air ingress during core degradation, Sandia National Laboratory, Report SAND2000-1935C, 2000, <https://digital.library.unt.edu/ark:/67531/metadc716516/>.
- Schanz, G., Adroguer, B., Volchek, A., 2004. Advanced treatment of zircaloy cladding high-temperature oxidation in severe accident code calculations. *Nucl. Eng. Des.* 232 (1), 75–84. <https://doi.org/10.1016/j.nucengdes.2004.02.013>.
- Schanz, G., Heck, M., Hózer, Z., Matus, L., Nagy, I., Sepold, L., Stegmaier, U., Steinbrück, M., Steiner, H., Stuckert, J., Windberg, P., 2006. Results of the QUENCH-10 experiment on air ingress. *Scient. Rep. FZKA-7087*. <https://doi.org/10.5445/IR/270064700>.
- Sepold, L., Hering, W., Homann, C., Miassoedov, A., Schanz, G., Stegmaier, U., Steinbrück, M., Steiner, H., Stuckert, J., 2004. Experimental and computational results of the QUENCH-06 test (OECD ISP-45). Scientific report FZKA-6664, Karlsruhe, February 2004, doi:10.5445/IR/270057214.
- Sepold, L., Schanz, G., Steinbrück, M., Stuckert, J., Miassoedov, A., Palagin, A., Veshchunov, M., 2006. Results of the QUENCH-09 experiment compared to QUENCH-07 with incorporation of B4C Absorber. *Nucl. Technol.* 154 (1), 107–116. <https://doi.org/10.13182/NT06-A3721>.
- Sepold, L., Lind, T., Csordás, A.P., Stegmaier, U., Steinbrück, M., Stuckert, J., 2009. AgInCd control rod failure in the QUENCH-13 bundle test. *Ann. Nucl. Energy* 36 (9), 1349–1359. <https://doi.org/10.1016/j.anucene.2009.06.020>.
- Steinbrück, M., 2009. Prototypical experiments relating to air oxidation of Zircaloy-4 at high temperatures. *J. Nucl. Mater.* 392 (3), 531–544. <https://doi.org/10.1016/j.jnucmat.2009.04.018>.
- Steinbrück, M., 2014. High-temperature reaction of oxygen-stabilized α -Zr(O) with nitrogen. *J. Nucl. Mater.* 447 (1–3), 46–55. <https://doi.org/10.1016/j.jnucmat.2013.12.024>.
- Steinbrück, M., Bottcher, M., 2011. Air oxidation of Zircaloy-4, M5® and ZIRLO™ cladding alloys at high temperatures. *J. Nucl. Mater.* 414 (2), 276–285. <https://doi.org/10.1016/j.jnucmat.2011.04.012>.
- Steinbrück, M., Schaffer, S., 2016. High-Temperature Oxidation of Zircaloy-4 in Oxygen-Nitrogen Mixtures. *Oxid. Met.* 85 (3–4), 245–262. <https://doi.org/10.1007/s11085-015-9572-1>.
- Steinbrück, M., Große, M., Sepold, L., Stuckert, J., 2010. Synopsis and outcome of the QUENCH experimental program. *Nucl. Eng. Des.* 240 (7), 1714–1727. <https://doi.org/10.1016/j.nucengdes.2010.03.021>.
- Steinbrück, M., da Silva, F.O., Grosse, M., 2017. Oxidation of Zircaloy-4 in steam-nitrogen mixtures at 600–1200 °C DOI. *J. Nucl. Mater.* 490, 226–237. <https://doi.org/10.1016/j.jnucmat.2017.04.034>.
- Stuckert, J., Birchley, J., Grosse, M., Jaeckel, B., Steinbrück, M., 2010. Experimental and calculation results of the integral reflood test QUENCH-14 with M5® cladding tubes. *Ann. Nucl. Energy* 37 (8), 1036–1047. <https://doi.org/10.1016/j.anucene.2010.04.015>.
- Stuckert, J., Birchley, J., Große, M., Jaeckel, B., Steinbrück, M., 2011. Experimental and calculation results of the integral reflood test QUENCH-15 with ZIRLO™ cladding tubes in comparison with results of previous QUENCH tests. *Nucl. Eng. Des.* 241 (8), 3224–3233. <https://doi.org/10.1016/j.nucengdes.2011.05.004>.
- Stuckert, J., Steinbrueck, M., Grosse, M., 2013. Experimental program QUENCH at KIT on core degradation during reflooding under LOCA conditions and in the early phase of a severe accident. Proceedings of Meeting on Modelling of Water Cooled Fuel Including Design Basis and Severe Accidents, Chengdu/China, 2013, IAEA TECDOC CD-1775, pp. 281–297, https://www.iaea.org/inis/collection/NCLCollectionStore/_Public/47/035/47035567.pdf?r=1.
- Stuckert, J., Hering, W., Sánchez-Espinoza, V., Tromm, W., 2019. Effect of core reflood on melt relocation. Final report Ares(2019)5357622, IVMR identification D3.14, 2019, <https://ec.europa.eu/research/participants/documents/downloadPublic?documentIds=080166e5c5a07064&appId=PPGMS>.
- Stuckert, J., Veshchunov, M., 2008. Behaviour of Oxide Layer of Zirconium-Based Fuel Rod Cladding under Steam Starvation Conditions. Scientific report FZKA-7373. <https://doi.org/10.5445/IR/270071587>.
- Stuckert, J., Hózer, Z., Kiselev, A., Steinbrück, M., 2016. Cladding oxidation during air ingress. Part I: experiments on air ingress. *Ann. Nucl. Energy* 93, 4–17. <https://doi.org/10.1016/j.anucene.2015.12.034>.
- Stuckert, J., Kalilainen, J., Lind, T., Stegmaier, U., Steinbrück, M., Zhang, Y., 2020. Results of the QUENCH-18 Bundle Experiment on Air Ingress and AgInCd absorber behavior. Scientific Report NUSAFE 3570. <https://doi.org/10.5445/IR/1000131350>.
- Stuckert, J., Steinbrück, M., 2014. Experimental results of the QUENCH-16 bundle test on air ingress. *Prog. Nucl. Energy* 71, 134–141. <https://doi.org/10.1016/j.pnucene.2013.12.001>.
- Stuckert, J., Grosse, M., Steinbrueck, M., Walter, M., Wensauer, A., 2020. Results of the QUENCH-LOCA experimental program at KIT. *J. Nucl. Mater.* 534, 152143. <https://doi.org/10.1016/j.jnucmat.2020.152143>.
- Uetsuka, H., Hofmann, P., 1985. Reaction Kinetics of Zircaloy-4 in a 25% O₂/75% Ar Gas Mixture from 900 to 1500°C under Isothermal Conditions. Scientific report KfK 3917. <https://doi.org/10.5445/IR/270021279>.
- Urbanic, V.F., Heidrick, T.R., 1978. High temperature oxidation of Zircaloy-2 and Zircaloy-4 in steam. *J. Nucl. Mater.* 75, 251–261. [https://doi.org/10.1016/0022-3115\(78\)90006-5](https://doi.org/10.1016/0022-3115(78)90006-5).
- Veshchunov, M. S., Stuckert, J., Berdyshev, A., 2002. Modelling of Zr-O and U-Zr-O melts oxidation and new crucible tests. Scientific Report FZKA-6792. doi:10.5445/IR/270053667.

Repository KITopen

Dies ist ein Postprint/begutachtetes Manuskript.

Empfohlene Zitierung:

Stuckert, J.; Steinbrueck, M.; Kalilainen, J.; Lind, T.; Birchley, J.
[Experimental and modelling results of the QUENCH-18 bundle experiment on air ingress, cladding melting and aerosol release.](#)
2021. Nuclear engineering and design, 379.
doi: [10.5445/IR/1000133354](https://doi.org/10.5445/IR/1000133354)

Zitierung der Originalveröffentlichung:

Stuckert, J.; Steinbrueck, M.; Kalilainen, J.; Lind, T.; Birchley, J.
[Experimental and modelling results of the QUENCH-18 bundle experiment on air ingress, cladding melting and aerosol release.](#)
2021. Nuclear engineering and design, 379, Art.-Nr.: 111267.
doi: [10.1016/j.nucengdes.2021.111267](https://doi.org/10.1016/j.nucengdes.2021.111267)

Lizenzinformationen: [CC BY-NC-ND 4.0](#)